electronics

MDPI

Article

Estimation of IQI for AF Cooperative Single-Carrier Frequency Domain Equalization Systems Using Channel Decoder Feedback

Mohamed Marey [1,*,†] and Hala Mostafa [2,†]

[1] Smart Systems Engineering Laboratory, College of Engineering, Prince Sultan University, Riyadh 11586, Saudi Arabia

[2] Department of Information Technology, College of Computer and Information Sciences, Princess Nourah bint Abdulrahman University, P.O. Box 84428, Riyadh 11671, Saudi Arabia

* Correspondence: mfmmarey@psu.edu.sa

† These authors contributed equally to this work.

Abstract: The process of amplify-and-forward (AF) relaying is essential to the improvement of both current and future wireless communication standards. Nevertheless, significant performance loss may be posed by in-phase and quadrature imbalance (IQI) caused by defects in radio frequency components. Prior studies into this research problem were restricted to uncoded broadcasts, even though error-correcting codes are frequently used in real applications. To this purpose, we develop a novel approach applicable to the destination terminal for estimating and compensating for IQI that occurs at the source, relay, and destination terminals. The proposed approach is explored in the context of coded emissions of AF single-carrier frequency domain equalization (SC-FDE) systems. In contrast to other methods for mitigating this radio frequency deflection at each node, the proposed system estimates and compensates for all IQI parameters and channel impulse responses simultaneously. With the use of an iterative expectation–maximization (EM) process, a maximum-likelihood (ML) solution to the problem is computed. At each round, the soft information supplied by the channel decoder is employed to create the *a posteriori* expectations of the sent data symbols, which are then fed into the estimation process as if they were training symbols. In addition, we address how to use the estimated parameters to perform the task of data detection. The offered predictor and detector exchange soft information in a sequential process, boosting the overall system effectiveness. The simulation results show that the proposed method is not only practicable but superior to the established methods.

Keywords: IQ imbalance; relaying transmissions; soft decoding process

Citation: Marey, M.; Mostafa, H. Estimation of IQI for AF Cooperative Single-Carrier Frequency Domain Equalization Systems Using Channel Decoder Feedback. *Electronics* **2023**, *12*, 863. https://doi.org/10.3390/electronics12040863

Academic Editors: Angela Digulescu, Roland Gautier, Florin Popescu and Annamaria Sarbu

Received: 17 January 2023
Revised: 3 February 2023
Accepted: 6 February 2023
Published: 8 February 2023

1. Introduction

Technology related to wireless communications has advanced at a pace that is incredibly rapid. Each successive version of wireless devices, despite being just a few years apart, has brought considerable advancements in connection communication speed, device dimensions, battery capacity, etc. Dealing with the unpredictability of fading channels is one of the most critical issues that must be overcome in order to accomplish the goal of providing trustable transmissions. Diversity is an efficient approach to alleviate the issue of fading in wireless links [1]. It allows for the use of several independently fading versions of the sent information, which increases transmission performance. Diversity could well be manifested in numerous manners, including temporal, frequency, and spatial diversity. The latter option could well be accomplished using multiple-input multiple-output (MIMO) technologies by deploying numerous antennas at the broadcaster and/or recipient side [2–4]. It is not feasible to use numerous antennas on portable terminals such as mobile phones and wireless sensor nodes. This is due to the constraints imposed by their size, power consumption, and cost.

In recent years, there has been growing interest in relay-assisted communications as a novel approach to attain diversity because of their potential to harness the benefits of spatial diversity and extended coverage [5,6]. This broadcast architecture produces a powerful virtual multi-antenna system, which aids in taking benefits of the wireless medium's transmission characteristics. Links can be made more resilient to wireless channel defects if several copies of the same sent information arrive at the recipient as a result of relaying. In addition, relaying information between nodes takes advantage of the nonlinear connection between distance and propagation loss, which reduces the overall signal attenuation. These improvements in signal robustness can lead to a decrease in transmitted power at the terminals. It should not come as a surprise that relaying protocols have found applications in a variety of wireless standards, including mobile, microwave, internet of things, and satellite systems [7–10].

A transmission protocol for relays specifies how a relay should handle data it receives from its upstream node. Several relay protocols have been covered in scholarly articles, such as amplify-and-forward (AF) and decode-and-forward (DF) [11,12]. When using an AF relaying system, the relay functions similarly to conventional analog repeaters. The source sends data to the receiver during the first time slot. Due to the transmission nature of the wireless channels, the relay also picks up the signal. After that, the relay amplifies the corrupted version of the source signal without decoding it, and re-sends it. This transmission protocol has less stringent hardware requirements since the relay is not responsible for decoding. In contrast, a DF relay serves as an intelligent repeater by first decoding the source signal before forwarding it to its intended recipient. The DF relay cannot interpret the incoming information correctly if the channel settings on the source-relay connection are poor. This restricts the efficiency of the DF protocols.

In addition, multicarrier broadcasts have been commonplace in the last couple of decades for the purpose of broadband communication in order to overcome frequency-selective fading channels. Orthogonal frequency division multiplexing (OFDM) technology plays an essential role in the development of wireless communication systems over frequency-selective fading channels. This is due to its capacity to offer a high data rate while also preserving a straightforward receiver design. The single-carrier frequency domain equalization (SC-FDE) approaches have also found widespread use in a variety of contemporary wireless communication systems. These systems include, for example, IEEE 802.11.ad and IEEE 802.16 Wimax [13]. To successfully apply low-complexity and precise frequency-domain channel equalization, an SC-FDE system typically utilizes a data structure consisting of data chunks, each preceded by a cyclic prefix. When compared to OFDM, SC-FDE excels because of its lower peak-to-average power ratio (PAPR) and less susceptibility to carrier-frequency offset [14].

At the same time, the direct conversion architecture has been recognized as one of the most potential radio designs for the development of both present and future wireless transceivers [15,16]. This, also known as zero-IF architecture, bypasses the need for intermediary frequency segments between the radio frequency (RF) and the baseband, and vice versa. There are several benefits, such as reduced size, cost, and power consumption. The deployment of direct conversion radios, on the other hand, is fraught with a variety of difficulties and technological obstacles. If everything went perfectly, the two local oscillator signals would be exactly 90 degrees out of phase with one another, have the same amplitude, and go through identical circuits in parallel. Even with the most advanced RF integrated circuit technology, the 90-degree phase shift and equal amplitudes of the in-phase (I) and quadrature (Q) signal channels can only be achieved to a certain degree of accuracy in real life. In addition, the frequency responses of the low-pass filters and amplifiers in the I and Q branches vary, which leads to overall amplitude and phase mismatches.

1.1. Relevant Works

Several works have examined the efficiency of relaying schemes, assuming a perfect RF front-end (e.g., see [17,18] and references therein). However, in reality, RF restrictions such as IQ imbalance (IQI), antenna coupling, phase-noise, and carrier-frequency misalignment all have a detrimental impact on relaying systems performance [19,20]. The majority of IQI research has been conducted in the context of single-hop wireless communications (e.g., see [21–24] and references therein). The influence of IQI on relaying systems has been the subject of fewer investigations. An analytical equation for the symbol error probability (SEP) was obtained in [25] across frequency-flat channels, taking into consideration dual-hop AF relaying with IQI present at the recipient terminal. Lower and upper constraints on the average SEP are given in the study that looked into the impacts of IQI in two-way AF relaying [26]. This study explored the effects of IQI at both the source and recipient terminals. Due to the low-quality hardware often found in inexpensive relay nodes, IQI is more likely to occur at the relay, which was not taken into account in [25,26]. Theoretical calculations for the outage probability and the error vector magnitude have been reported in [27], which provides more detail on the impacts of IQI at the AF relay terminal in orthogonal frequency division multiplexing (OFDM) transmissions. Notably, the authors of [27] demonstrated that flawless single-hop systems can surpass AF transmissions with low IQI levels. After taking IQI at the relay node into consideration, revised mathematical formulas for the outage probability and ergodic capacity were developed over in m-Nakagami fading channels [28]. The detrimental impacts of IQI, which are emphasized in terms of signal-to-interference, on the behaviors of dual-hop channel state information-assisted AF relaying are discussed in [29]. In addition, the authors of [29] suggested two compensation algorithms to identify the transmitted signal, with the ML design being the greatest at limiting the impacts of IQI despite the increased complication. The outage probabilities for variable-gain AF and DF, which are affected by both IQI and additive hardware limitation, have been determined in [30], as well as their optimal detectors. In [31], a comprehensive sum rate study has been performed to assess the influence of IQI in both the transmitter and the receiver on the generalized frequency division multiplexing wireless transmissions, and a compensatory mechanism based on pilots has been presented. An intriguing correlation between IQI and residual self-interference in a full-duplex AF relaying network has been emphasized in [32]. Two IQI compensation algorithms with channel awareness have been designed in [33,34] for use in DF multicarrier two-path consecutive relay schemes.

1.2. Novelties and Contributions

The purpose of this research is to design and examine a novel prediction and compensation algorithm for IQI in AF relaying SC-FDE systems operating on unknown multipath wireless channels. The following bullets provide a summary of the most significant novelties and contributions made by the article.

- Each of the previously reported works adopted a variety of algorithms to estimate and adjust for IQI at each wireless network node, as well as additional algorithms to estimate and equalize fading wireless channels. This article aggregates the impacts of IQI occurring at the source, relay, and destination nodes, as well as the channel impulse responses (CIRs) across nodes, into two unknown elements termed the equivalent CIR.
- At the destination node, we create a novel algorithm to estimate the equivalent CIR using maximum-likelihood (ML) concepts. We utilize an expectation–maximization (EM) [35,36] procedure for a straightforward implementation of the offered ML algorithm.
- Previous investigations of this research problem were only conducted using uncoded broadcasts. However, error-control codes are extensively used in a variety of practical applications. In this work, the soft outputs of an error-control code decoder are used to compute the a posteriori expectations of the data symbols, which are then engaged as training symbols by the offered estimator.
- We illustrate how the decoding process is carried out using the prediction of equivalent CIR.

The following is a description of the structure of the remaining parts of the work. The SC-FDE AF system model under consideration is discussed in Section 2. Section 3 explains the suggested estimation method, while Section 4 addresses the proposed data detection strategy. Section 5 includes the simulation results and an appropriate analysis. In the last step, the study is summarized in Section 6.

2. System Description

In particular, we are interested in a relaying system shown in Figure 1 with three stations: the source (S), the relay (R), and the destination (D). The R node uses AF relaying and functions in half-duplex mode, which means that sending and receiving happen at different times. We suppose that each data transfer takes place in discrete units called packets. The source, using an error-correcting encoder, converts a series of B binary bits into C coded bits. Interleaving the encoder's output bits is the first step in transforming them into a vector of N data symbols using a digital modulator. The interleaver is a crucial component because it allows error bursts to be dispersed over numerous codewords, which can then be corrected by channel decoders. Each symbol is part of the signaling pattern Φ, $N = C/\log_2\langle\Phi\rangle$, where $\langle\Phi\rangle$ reflects the cardinality of Φ. To that end, $\mathbf{a} = [a(N-2-\nu), \ldots, a(N-1), a(0), a(1), \ldots, a(N-1)]^\dagger$ represents the sent packet. Here, $a(n)$ is the nth data symbol, $\dagger$ stands for the vector-transpose operator, and ν samples are included as a cyclic prefix to counteract the inter-symbol interference caused by wireless channels. The baseband version of the up-converted stream that was broadcast by the source in the presence of IQI can be described as

$$\overline{\mathbf{a}} = g_S\mathbf{a} + f_S\mathbf{a}^*, \tag{1}$$

where * represents the complex-conjugate action, and g_S and f_S are provided as [21,22]

$$g_S = \cos(\theta_S) + j\beta_S\sin(\theta_S), \tag{2}$$

$$f_S = \beta_S\cos(\theta_S) + j\sin(\theta_S). \tag{3}$$

Here, β_S and ϑ_S model the source amplitude and the phase differences between the I and Q routes, and $j = \sqrt{-1}$. It usually takes two passes to complete the packet delivery. In the first pass, both R and D nodes receive the sent signal. We define $\mathbf{h}_{SR} = [h_{SR}(0), \ldots, h_{SR}(L-1)]^\dagger$ and $\mathbf{h}_{SD} = [h_{SD}(0), \ldots, h_{SD}(L-1)]^\dagger$ as the time-domain representations of the frequency-selective connections between S and R, and S and D, respectively, with L being the number of channel taps. The packets acquired at the R and D nodes are given as

$$\mathbf{z}_R = \overline{\mathbf{a}} \otimes \mathbf{h}_{SR} + \mathbf{n}_R, \tag{4}$$

$$\mathbf{z}_D^{(1)} = \overline{\mathbf{a}} \otimes \mathbf{h}_{SD} + \mathbf{n}_D^{(1)}, \tag{5}$$

where $\otimes$ refers to the linear convolution action, and $\mathbf{n}_R$ and $\mathbf{n}_D^{(1)}$ are the noise contributions at the R and D nodes, respectively. When we impose the influence of the relay's IQI on $\mathbf{z}_R$ and the destination's IQI on $\mathbf{z}_D^{(1)}$, we obtain

$$\overline{\mathbf{z}}_R = g_{R1}\mathbf{z}_R + f_{R1}\mathbf{z}_R^*, \tag{6}$$

$$\overline{\mathbf{z}}_D^{(1)} = g_D\mathbf{z}_D^{(1)} + f_D\mathbf{z}_D^{(1)*}, \tag{7}$$

where g_{R1}, f_{R1}, g_D, and f_D are described, as shown in (2) and (3), replacing S with $R1$ and D. In the second pass, the received signal undergoes a transformation at the R station, which is then conveyed to the D node. The signal sent by the R node is expressed as

$$\overline{\mathbf{x}}_R = \psi(g_{R2}\overline{\mathbf{z}}_R + f_{R2}\overline{\mathbf{z}}_R^*), \tag{8}$$

where g_{R2} and f_{R2} are the IQI parameters of the transmit part of the relay, and ψ is the scaling factor provided as [37]

$$\psi = \frac{1}{\sqrt{\sum_{l=0}^{L-1} |h_{SR}(l)|^2 + \sigma_n^2}}. \tag{9}$$

Here, σ_n^2 is the noise variance. The signal gathered at the destination is then written as

$$\overline{\mathbf{z}}_D^{(2)} = \overline{\mathbf{x}}_R \otimes \mathbf{h}_{RD} + \mathbf{n}_D^{(2)}, \tag{10}$$

where $\mathbf{h}_{RD} = [h_{RD}(0), \ldots, h_{RD}(L-1)]^\dagger$ is the multipath channel coefficients of link between R and D terminals, and $\mathbf{n}_D^{(2)}$ is the corresponding noise samples. The consequence of adding the destination's IQI effect on $\mathbf{z}_D^{(2)}$ is

$$\overline{\mathbf{z}}_D^{(2)} = g_D \mathbf{z}_D^{(2)} + f_D \mathbf{z}_D^{(2)*}. \tag{11}$$

The study's objective is to find a way to estimate all unknowns of $\mathbf{h}_{SR}$, $\mathbf{h}_{SD}$, $\mathbf{h}_{RD}$, g_S, f_S, g_{R1}, f_{R1}, g_{R2}, f_{R2}, g_D, and f_D at the same time as well as developing a data detection scheme.

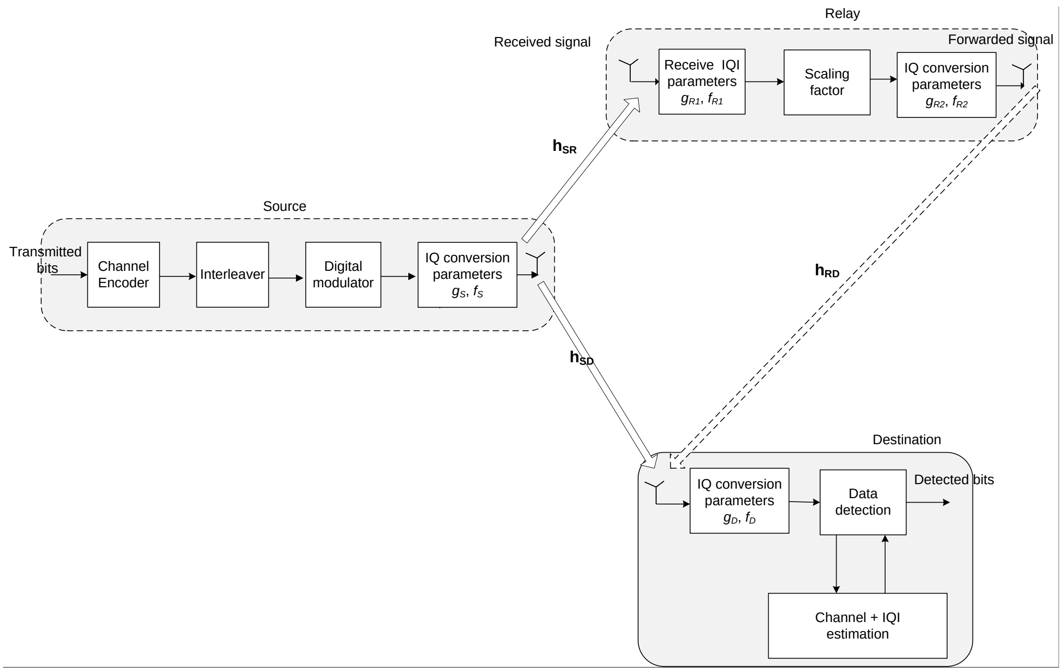

Figure 1. The principal structure of S, R, and D terminals. The solid arrows indicate broadcasts during the first pass and the dashed arrow describes broadcasts during the second one.

3. Proposed Estimation Algorithm

The key role of the destination is to extract the information sent by the source using the investigations of $\overline{\mathbf{z}}_D^{(1)}$ and $\overline{\mathbf{z}}_D^{(2)}$. Clearly, it is essential to extract the IQI parameters introduced at the S, R, and D nodes, as well as the channel coefficients between the different terminals. We can tackle the issue at hand by reforming the earlier equations. Utilizing (1) and (4)–(7) and conducting few simple mathematical computations, we write $\overline{\mathbf{z}}_D^{(1)}$ as

$$\overline{\mathbf{z}}_D^{(1)} = \overline{\mathbf{A}}^{(1)} \mathbf{H}_{SD} + \mathbf{n}_D^{(1)}, \tag{12}$$

where $\overline{\mathbf{A}}^{(1)} = [\mathbf{A}, \mathbf{A}, \mathbf{A}^*, \mathbf{A}^*]$ and $\mathbf{H}_{SD} = \left[\mathbf{h}_{SD}^{(1)\dagger}, \mathbf{h}_{SD}^{(2)\dagger}, \mathbf{h}_{SD}^{(3)\dagger}, \mathbf{h}_{SD}^{(4)\dagger}\right]^\dagger$. Here,

$$\mathbf{h}_{SD}^{(1)} = g_D g_S \mathbf{h}_{SD}, \tag{13a}$$

$$\mathbf{h}_{SD}^{(2)} = f_D f_S^* \mathbf{h}_{SD}^*, \tag{13b}$$

$$\mathbf{h}_{SD}^{(3)} = g_D f_S \mathbf{h}_{SD}, \tag{13c}$$

$$\mathbf{h}_{SD}^{(4)} = f_D f_S^* \mathbf{h}_{SD}^*, \tag{13d}$$

$\mathbf{A}$ is described as an $(N+L-1) \times (L-1)$ transmission matrix that can be created as

$$\mathbf{A} = \begin{bmatrix} a_0 & 0 & 0 & 0 & 0 \\ a_1 & a_0 & 0 & 0 & 0 \\ a_2 & a_1 & a_0 & 0 & 0 \\ \vdots & \vdots & \vdots & \vdots & \vdots \\ a_N & a_{N-1} & a_{N-2} & \dots & a_{N-L-1} \\ 0 & x_N & x_{N-1} & \dots & x_{N-L-2} \\ \vdots & \vdots & \vdots & \vdots & \vdots \\ 0 & 0 & 0 & 0 & x_N \end{bmatrix}. \tag{14}$$

Using an analogous principle, $\overline{\mathbf{z}}_D^{(2)}$ is expressed as

$$\overline{\mathbf{z}}_D^{(2)} = \overline{\mathbf{A}}^{(2)} \mathbf{h}_{SRD} + \mathbf{n}_D^{(2)}, \tag{15}$$

where $\overline{\mathbf{A}}^{(2)} = [\mathbf{A}, \mathbf{A}, \mathbf{A}, \mathbf{A}, \mathbf{A}^*, \mathbf{A}^*, \mathbf{A}^*, \mathbf{A}^*]$ and $\mathbf{H}_{SRD} = \left[\mathbf{h}_{SRD}^{(1)\dagger}, \mathbf{h}_{SRD}^{(2)\dagger}, \dots, \mathbf{h}_{SD}^{(8)\dagger}\right]^\dagger$. Here,

$$\mathbf{h}_{SRD}^{(1)} = \psi g_S g_D (g_{R1} g_{R2} + f_{R1}^* f_{R2}) \mathbf{h}_{SR} \otimes \mathbf{h}_{RD}, \tag{16a}$$

$$\mathbf{h}_{SRD}^{(2)} = \psi f_S g_D (g_{R2} f_{R1} + f_{R2} g_{R1}^*) \mathbf{h}_{SR}^* \otimes \mathbf{h}_{RD}, \tag{16b}$$

$$\mathbf{h}_{SRD}^{(3)} = \psi f_S^* f_D (g_{R1}^* g_{R2}^* + f_{R1} f_{R2}^*) \mathbf{h}_{SR}^* \otimes \mathbf{h}_{RD}^*, \tag{16c}$$

$$\mathbf{h}_{SRD}^{(4)} = \psi g_S f_D (f_{R1}^* g_{R2}^* + g_{R1} f_{R2}^*) \mathbf{h}_{SR} \otimes \mathbf{h}_{RD}^*, \tag{16d}$$

$$\mathbf{h}_{SRD}^{(5)} = \psi g_S g_D (g_{R2} g_{R1} + f_{R2} f_{R1}^*) \mathbf{h}_{SR}^* \otimes \mathbf{h}_{RD}, \tag{16e}$$

$$\mathbf{h}_{SRD}^{(6)} = \psi g_S^* g_D (g_{R2} f_{R1} + f_{R2} g_{R1}^*) \mathbf{h}_{SR}^* \otimes \mathbf{h}_{RD}, \tag{16f}$$

$$\mathbf{h}_{SRD}^{(7)} = \psi g_S^* f_D (g_{R1}^* g_{R2}^* + f_{R2}^* f_{R1}) \mathbf{h}_{SR}^* \otimes \mathbf{h}_{RD}^*, \tag{16g}$$

$$\mathbf{h}_{SRD}^{(8)} = \psi g_S^* f_D (f_{R1}^* g_{R2}^* + f_{R2}^* g_{R1}) \mathbf{h}_{SR} \otimes \mathbf{h}_{RD}^*. \tag{16h}$$

The above arrangements of (12) and (15) permit the estimation of two components, $\mathbf{H}_{SD}$ and $\mathbf{H}_{SRD}$, as opposed to the eleven variables of $\mathbf{h}_{SR}$, $\mathbf{h}_{SD}$, $\mathbf{h}_{RD}$, g_S, f_S, g_{R1}, f_{R1}, g_{R2}, f_{R2}, g_D, and f_D. The ML predictions of $\mathbf{H}_{SD}$ and $\mathbf{H}_{SRD}$ are obtained by maximizing the log-likelihood function as follows:

$$\begin{aligned} \left[\hat{\mathbf{H}}_{SD}, \hat{\mathbf{H}}_{SRD}\right] = \arg \max_{\mathbf{H}_{SD}, \mathbf{H}_{SRD}} \log \\ \Pr\left(\overline{\mathbf{z}}_D^{(1)}, \overline{\mathbf{z}}_D^{(2)} \middle| \overline{\mathbf{A}}^{(1)}, \overline{\mathbf{A}}^{(2)}, \mathbf{H}_{SD}, \mathbf{H}_{SRD}\right), \end{aligned} \tag{17}$$

where $\Pr\ (\diamond|\triangleleft)$ is defined as the probability density function of $\diamond$ given $\triangleleft$, and $\hat{\diamond}$ is the calculated value of $\diamond$. Since $\overline{\mathbf{z}}_D^{(1)}$ and $\overline{\mathbf{z}}_D^{(2)}$ are independent sequences, we compose

$$\begin{aligned} \Pr\left(\overline{\mathbf{z}}_D^{(1)}, \overline{\mathbf{z}}_D^{(2)} \middle| \overline{\mathbf{A}}^{(1)}, \overline{\mathbf{A}}^{(2)}, \mathbf{H}_{SD}, \mathbf{H}_{SRD}\right) = \\ \Pr\left(\mathbf{z}_D^{(1)} \middle| \overline{\mathbf{A}}^{(1)}, \mathbf{H}_{SD}\right) \Pr\left(\overline{\mathbf{z}}_D^{(2)} \middle| \overline{\mathbf{A}}^{(2)}, \mathbf{H}_{SRD}\right), \end{aligned} \tag{18}$$

where
$$\Pr\left(\overline{\mathbf{z}}_D^{(1)}\middle|\overline{\mathbf{A}}^{(1)},\mathbf{H}_{SD}\right)\propto\exp\left(\frac{-1}{\sigma_n^2}\left\|\overline{\mathbf{z}}_D^{(1)}-\overline{\mathbf{A}}^{(1)}\mathbf{H}_{SD}\right\|^2\right),\tag{19}$$
and
$$\Pr\left(\overline{\mathbf{z}}_D^{(2)}\middle|\overline{\mathbf{A}}^{(2)},\mathbf{H}_{SRD}\right)\propto\exp\left(\frac{-1}{\sigma_n^2}\left\|\overline{\mathbf{z}}_D^{(2)}-\overline{\mathbf{A}}^{(2)}\mathbf{H}_{SRD}\right\|^2\right).\tag{20}$$
As indicated in (17)–(20), the accurate ML approach demands prior information of the matrices $\overline{\mathbf{A}}^{(1)}$ and $\overline{\mathbf{A}}^{(2)}$, which are generally inaccessible. In circumstances like these, when nuisance parameters are prominent, the EM system delivers a solution that comprises multiple rounds of searching for the ML predictions [35,36]. During each round of the process, the system switches back and forth between what is known as an expectation step (E-step) and a maximization step (M-step). The former provides a numerical evaluation of the conditional probability of the examined signal, given the present measurements of the unknown parameters. In order to acquire updated estimates for the unknowable parameters, the latter maximizes the amount obtained in the E-step. The mathematical representation of the E-step at round ι is

$$\begin{aligned}&\mathrm{U}\left([\mathbf{H}_{SD},\mathbf{H}_{SRD}]\middle|\left[\hat{\mathbf{H}}_{SD}(\iota),\hat{\mathbf{H}}_{SRD}(\iota)\right]\right)=\\&\mathrm{E}\Big[\log\Pr\left(\overline{\mathbf{z}}_D^{(1)},\overline{\mathbf{z}}_D^{(2)}\middle|\overline{\mathbf{A}}^{(1)},\overline{\mathbf{A}}^{(2)},\mathbf{H}_{SD},\mathbf{H}_{SRD}\right)\Big|\overline{\mathbf{z}}_D^{(1)},\\&\qquad\overline{\mathbf{z}}_D^{(2)},\hat{\mathbf{H}}_{SD}(\iota),\hat{\mathbf{H}}_{SRD}(\iota)\Big]\\&=\int_{\overline{\mathbf{A}}^{(1)},\overline{\mathbf{A}}^{(2)}}\log\Pr\left(\overline{\mathbf{z}}_D^{(1)},\overline{\mathbf{z}}_D^{(2)}\middle|\overline{\mathbf{A}}^{(1)},\overline{\mathbf{A}}^{(2)},\mathbf{H}_{SD},\mathbf{H}_{SRD}\right)\times\\&\Pr\left(\overline{\mathbf{A}}^{(1)},\overline{\mathbf{A}}^{(2)}\middle|\overline{\mathbf{z}}_D^{(1)},\overline{\mathbf{z}}_D^{(2)},\hat{\mathbf{H}}_{SD}(\iota),\hat{\mathbf{H}}_{SRD}(\iota)\right)d\overline{\mathbf{A}}^{(1)}d\overline{\mathbf{A}}^{(2)},\end{aligned}\tag{21}$$

where the expectation is realized over $\overline{\mathbf{A}}^{(1)}$ and $\overline{\mathbf{A}}^{(2)}$. As a result, we derive the M-step as

$$\begin{aligned}\left[\hat{\mathbf{H}}_{SD}(\iota+1),\hat{\mathbf{H}}_{SRD}(\iota+1)\right]=\arg\max_{\mathbf{H}_{SD},\mathbf{H}_{SRD}}\\\mathrm{U}\left([\mathbf{H}_{SD},\mathbf{H}_{SRD}]\middle|\left[\hat{\mathbf{H}}_{SD}(\iota),\hat{\mathbf{H}}_{SRD}(\iota)\right]\right).\end{aligned}\tag{22}$$

Plugging (18)–(20) into (21) while disregarding the insignificant factors, we obtain

$$\begin{aligned}&\mathrm{U}\left([\mathbf{H}_{SD},\mathbf{H}_{SRD}]\middle|\left[\hat{\mathbf{H}}_{SD}(\iota),\hat{\mathbf{H}}_{SRD}(\iota)\right]\right)\propto\\&\quad 2\Re\left(\overline{\mathbf{z}}_D^{(1)\ddagger}\mathbf{Q}_1\mathbf{H}_{SD}\right)-\mathbf{H}_{SD}^{\ddagger}\mathbf{Q}_2\mathbf{H}_{SD}\\&\quad+2\Re\left(\overline{\mathbf{z}}_D^{(2)\ddagger}\mathbf{Q}_3\mathbf{H}_{SRD}\right)-\mathbf{H}_{SRD}^{\ddagger}\mathbf{Q}_4\mathbf{H}_{SRD},\end{aligned}\tag{23}$$

where the superscript ‡ represents the vector-transpose conjugate of a vector, and

$$\mathbf{Q}_1=\int\overline{\mathbf{A}}^{(1)}\Pr\left(\overline{\mathbf{A}}^{(1)}\middle|\overline{\mathbf{z}}_D^{(1)},\hat{\mathbf{H}}_{SD}(\iota)\right)d\overline{\mathbf{A}}^{(1)},\tag{24a}$$

$$\mathbf{Q}_2=\int\overline{\mathbf{A}}^{(1)\ddagger}\overline{\mathbf{A}}^{(1)}\Pr\left(\overline{\mathbf{A}}^{(1)}\middle|\overline{\mathbf{z}}_D^{(1)},\hat{\mathbf{H}}_{SD}(\iota)\right)d\overline{\mathbf{A}}^{(1)},\tag{24b}$$

$$\mathbf{Q}_3=\int\overline{\mathbf{A}}^{(2)}\Pr\left(\overline{\mathbf{A}}^{(2)}\middle|\overline{\mathbf{z}}_D^{(2)},\hat{\mathbf{H}}_{SRD}(\iota)\right)d\overline{\mathbf{A}}^{(2)},\tag{24c}$$

$$\mathbf{Q}_4=\int\overline{\mathbf{A}}^{(2)\ddagger}\overline{\mathbf{A}}^{(2)}\Pr\left(\overline{\mathbf{A}}^{(2)}\middle|\overline{\mathbf{z}}_D^{(2)},\hat{\mathbf{H}}_{SRD}(\iota)\right)d\overline{\mathbf{A}}^{(1)}.\tag{24d}$$

By setting the gradient of (23) with regard to $\mathbf{H}_{SD}$ and $\mathbf{H}_{SRD}$ to zero, the updated predictions are
$$\hat{\mathbf{H}}_{SD}(\iota+1)=\mathbf{Q}_2^{-1}\mathbf{Q}_1\overline{\mathbf{z}}_D^{(1)},\tag{25a}$$

$$\hat{\mathbf{H}}_{SRD}(\iota+1) = \mathbf{Q}_4^{-1}\mathbf{Q}_3\bar{\mathbf{z}}_D^{(2)}. \tag{25b}$$

The following points merit serious attention.

- The next issue that arises is how to truly find out what the matrices of $\mathbf{Q}_1$, $\mathbf{Q}_2$, $\mathbf{Q}_3$ and $\mathbf{Q}_4$ are in the real world. One expresses the a posteriori expectation of a transmitted symbol $a(k)$ as
$$\mathrm{E}[a(k)] = \sum_{\omega\in\Phi} \Pr\Big(a(k)=\omega \mid \bar{\mathbf{z}}_D^{(1)}, \bar{\mathbf{z}}_D^{(2)}, \hat{\mathbf{H}}_{SD}(\iota), \hat{\mathbf{H}}_{SRD}(\iota)\Big). \tag{26}$$
Therefore, the a posteriori expectation of the matrix $\mathbf{A}$ shown in (14) is created by swapping each matrix component with its associated a posteriori expectation calculated in (26). As a result, the matrices of $\mathbf{Q}_1$ and $\mathbf{Q}_3$ may be simply formed as $\mathbf{Q}_1 = [\tilde{\mathbf{A}}, \tilde{\mathbf{A}}, \tilde{\mathbf{A}}^*, \tilde{\mathbf{A}}^*]$ and $\mathbf{Q}_3 = [\tilde{\mathbf{A}}, \tilde{\mathbf{A}}, \tilde{\mathbf{A}}, \tilde{\mathbf{A}}, \tilde{\mathbf{A}}^*, \tilde{\mathbf{A}}^*, \tilde{\mathbf{A}}^*, \tilde{\mathbf{A}}^*]$, where $\tilde{\mathbf{A}}$ represents the a posteriori expectation of the matrix $\mathbf{A}$.
- In line with the widely held belief that data symbols are not independent from one another, it is easy to show that $\mathbf{Q}_3$ and $\mathbf{Q}_4$ are fairly portrayed by $\mathbf{Q}_1^{\dagger}\mathbf{Q}_1$ and $\mathbf{Q}_3^{\dagger}\mathbf{Q}_3$, respectively.
- It is important to recompute the a posteriori probability $\Pr\Big(a(k)=\omega \mid \bar{\mathbf{z}}_D^{(1)}, \bar{\mathbf{z}}_D^{(2)}, \hat{\mathbf{H}}_{SD}(\iota), \hat{\mathbf{H}}_{SRD}(\iota)\Big)$, and after each instance, we make a change to $\hat{\mathbf{H}}_{SD}(\iota)$ and $\hat{\mathbf{H}}_{SRD}(\iota)$). This entails restarting the channel decoder, which significantly complicates data processing. We utilize the embedded estimating technique [33,34] to avoid this computational cost. When $\hat{\mathbf{H}}_{SD}(\iota)$ and $\hat{\mathbf{H}}_{SRD}(\iota)$ are adjusted, the channel decoder is not rebooted; instead, it preserves the extrinsic and a priori probabilities computed during the last round of the channel decoder. In this case, the cost of the suggested EM estimation method is simplified.
- The preliminary settings for $\mathbf{H}_{SD}$ and $\mathbf{H}_{SRD}$ are drawn from (25a) and (25b) by adjusting the matrices of the $\mathbf{Q}_1$, $\mathbf{Q}_2$, $\mathbf{Q}_3$ and $\mathbf{Q}_4$ to simply the training symbols involvement.

4. Proposed Detector

First, the ν samples that match the cyclic prefix are deleted, enabling N samples to be evaluated further. Following a thorough inspection of (12) and (15), the outputs of the FFT unit at the kth and $-k$th bins are expressed as

$$r_1(k) = H_1(k)a(k) + H_2^*(-k)a^*(-k) + W_1(k), \tag{27a}$$

$$r_2(k) = H_3(k)a(k) + H_4^*(-k)a^*(-k) + W_2(k), \tag{27b}$$

where $W_1(k)$ and $W_2(k)$ are the corresponding noise factors, and $H_i(k)$ is the frequency domain channel coefficient, $i = 1, \ldots, 4$. Using (12) and (15), we express $H_i(k)$ as the kth output of the FFT unit used to process $\mathbf{h}_i$ as an input, where

$$\mathbf{h}_1 = \mathbf{h}_{SD}^{(1)} + \mathbf{h}_{SD}^{(2)}, \tag{28a}$$

$$\mathbf{h}_2 = \mathbf{h}_{SD}^{(3)} + \mathbf{h}_{SD}^{(4)}, \tag{28b}$$

$$\mathbf{h}_3 = \mathbf{h}_{SRD}^{(1)} + \mathbf{h}_{SRD}^{(2)} + \mathbf{h}_{SRD}^{(3)} + \mathbf{h}_{SRD}^{(4)}, \tag{28c}$$

$$\mathbf{h}_4 = \mathbf{h}_{SRD}^{(5)} + \mathbf{h}_{SRD}^{(6)} + \mathbf{h}_{SRD}^{(7)} + \mathbf{h}_{SRD}^{(8)}. \tag{28d}$$

We write (27a) and (27b) in a vector format as

$$\mathbf{r}(k) = \mathbf{H}(k)\mathbf{a}_1(k) + \mathbf{W}(k), \tag{29}$$

where $\mathbf{r}(k) = [r_1(k), r_2(k)]^{\dagger}$, $\mathbf{a}_1(k) = [a(k), a^*(-k)]^{\dagger}$, and

$$\mathbf{H}(k) = \begin{bmatrix} H_1(k) & H_2^*(-k) \\ H_3(k) & H_4^*(-k) \end{bmatrix}. \tag{30}$$

The a posteriori probability of $\mathbf{a}(k)$ is obtained as

$$\Pr(\mathbf{a}(k)|\mathbf{r}(k), \mathbf{H}(k)) \propto \exp\left(\frac{-1}{\sigma_n^2}\|\mathbf{r}(k) - \mathbf{H}(k)\mathbf{a}_1(k)\|^2\right)\Pr(a(k))\Pr(a^*(-k)). \tag{31}$$

We denote $\mathcal{L}[\cdot]$ as the label function and $b(k,m)$ is the mth bit of the data symbol $a(k)$. Accordingly, the bit metric $\lambda(b(k,m) = o)$, for $o = 0,1$, is calculated as

$$\lambda(b(k,m) = o) = \sum_{a^*(-k)\in\Phi} \sum_{\vartheta = F(o,m)} \Pr(\mathbf{a}_1(k)|\mathbf{r}(k), \mathbf{H}(k)), \tag{32}$$

where

$$F(o,m) = \mathcal{L}\left\{[b(k,0), \ldots, b(k, \log_2\langle\Phi\rangle - 1)] \middle| b(k,m) = o\right\}. \tag{33}$$

After de-interleaving, the bit metrics are sent into the decoder to determine the a posteriori probability of coded digits. The probabilities are then interleaved and delivered to the data symbol of the a posteriori computation unit. These probabilities are sent into the proposed estimator as a priori knowledge, as illustrated in (25a), (25b) and (31), respectively. The decoder utilizes the a posteriori probability of the transmitted bits to make hard judgments in the final round. The architectural schematic diagram of the intended detection and estimation processes is shown in Figure 2.

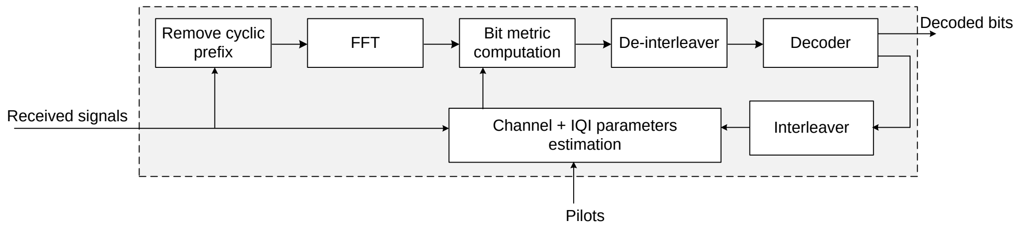

Figure 2. The block diagram of the suggested approach at the destination.

5. Simulation Results

We performed Monte Carlo simulations to validate the effectiveness of the proposed methods. Unless otherwise indicated explicitly, the following system parameters were used throughout simulations. A random interleaver and a 0.5-rate convolutional code with a constraint length of 8 and polynomials of 25 and 38 were considered. Set-partition mapping was utilized to convert the coded bits onto 16-QAM data symbols. Transmission packets of 964 data symbols were generated. A training sequence of length 60 was included in each packet to enable exploratory parameter prediction. A cyclic prefix of 10 samples was attached in each packet. The wireless link between any two nodes was characterized using eleven paths, $h_{\lambda_1\lambda_2}(l)$; each of them was a complex zero-mean Gaussian random variable with variance [38,39],

$$\sigma_{\lambda_1\lambda_2}(l) = \Upsilon_{\lambda_1\lambda_2}\exp(-l/11), \quad l = 0, \ldots, 9, \tag{34}$$

where λ_1 and $\lambda_2 \in \{S, R, D\}$, and $\Upsilon_{\lambda_1\lambda_2}$ was selected in a way that would result in each sub-carrier having an average energy of $\Lambda_{\lambda_1\lambda_2}$. We set $\Lambda_{SD} = 1$, $\Lambda_{SR} = 2.1$, and $\Lambda_{RD} = 1.8$. The channel coefficients are chosen independently for each packet simulated. The IQI parameters are $\rho_S = 0.91$, $\theta_S = 10^o$, $\rho_{R1} = 0.89$, $\theta_{R1} = 20^o$, $\rho_{R2} = 0.94$, $\theta_{R2} = 80^o$ and $\rho_D = 0.96$, $\theta_D = 12^o$. The signal-to-noise ratio (SNR) is defined as [29]

$$\text{SNR} = \frac{1}{\sigma_n^2}\left(\sum_l \mathrm{E}\left[|\mathbf{H}_{SD}(l)|^2 + |\mathbf{H}_{SRD}(l)|^2\right]\right). \tag{35}$$

Figure 3 illustrates the bit-error-rate (BER) of the offered approach as a function of the SNR. As can be seen, the BER performance keeps improving as the round process goes on. There is essentially no more performance gain beyond round seven. The cause for this behavior is explained as follows. Because the estimation technique is centered on a limited number of pilots, the soft information provided by the supplied detector is unreliable in the first round. However, as the number of rounds increases, more information is employed, leading to greater accuracy in both predictions and data detection, as compared to the data-aided case. There is essentially no more performance gain beyond round seven.

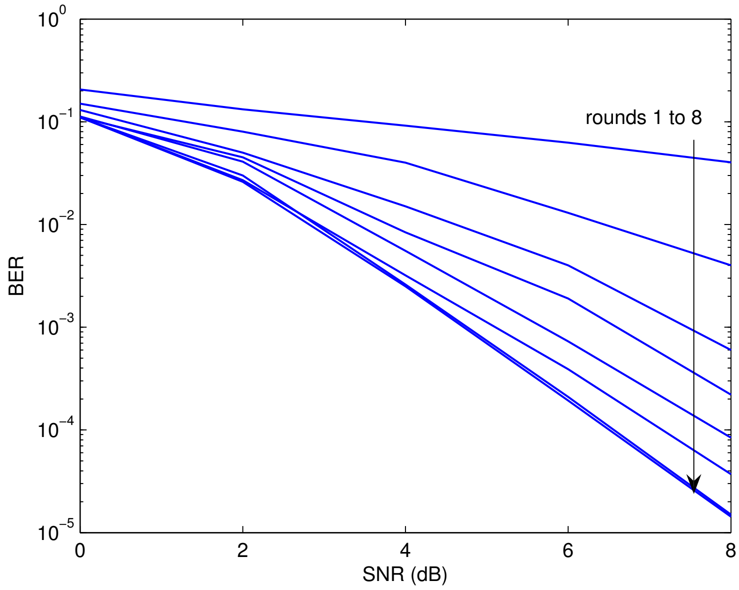

Figure 3. BER of the proposed approach.

Figure 4 compares the BER performance of the suggested design to that of other systems. There are two possible cases here: one in which the IQI is perfectly predicted and adjusted for, and another in which no IQI compensation is made at all. As can be observed, IQI results in poor BER performance if not corrected for. Clearly, the given method at round 8 has much better BER performance than that reported in [31,32], as well as approaches around 1 dB of the ideal performance of having complete knowledge of the channel and IQ parameters. This demonstrates that the offered strategy is successful.

Figure 5 highlights the BER performance of the offered approach for a family of QAM modulation formats with orders of 4, 16, 64, and 128 and round 8. When a higher-order modulation form is used, a decrease in BER performance can be seen. This is owing to the fact that the soft information findings of the channel decoder are less faithful as a consequence of utilizing a higher-order modulation scheme, which in turn has a bad influence on the BER performance.

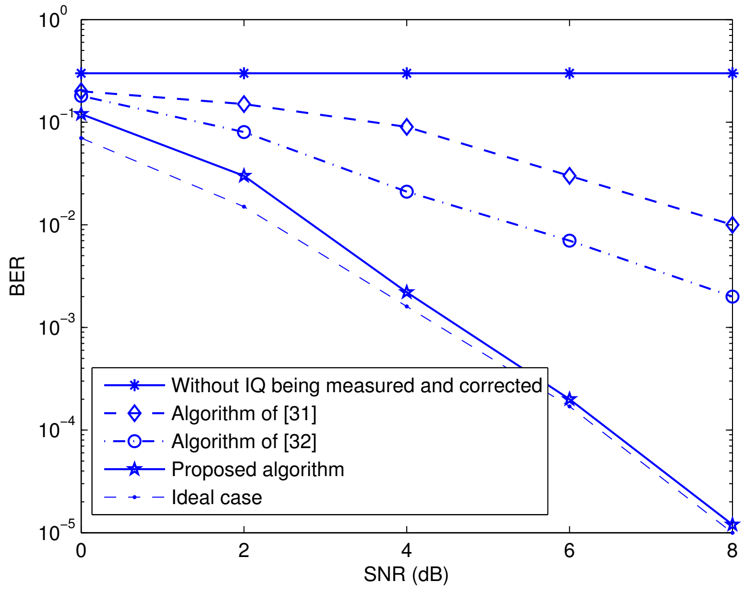

Figure 4. Comparative analysis of the BER performance of several systems.

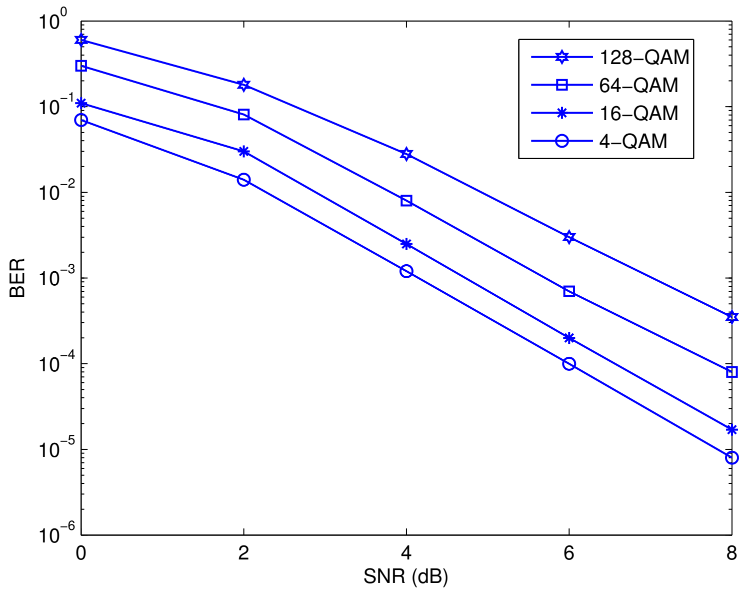

Figure 5. BER performance of the proposed approach at different modulation formats.

Figure 6 presents the BER performance of the offered architecture in two different implementations, one of which uses a convolutional code, and the other utilizes a turbo code. Here, the adopted turbo code has a rate of 1/2 and a constraint length of 8, including two convolutional codes [40]. It is well-known that turbo codes deliver more precise a posteriori expectations of the broadcast information compared to convolution codes, provided that both types of codes have identical parameters for code rate and constraint length [41]. Due to this fact, the results reveal that the BER performance of the proposed design improves with the use of a turbo code, as compared to a convolutional code.

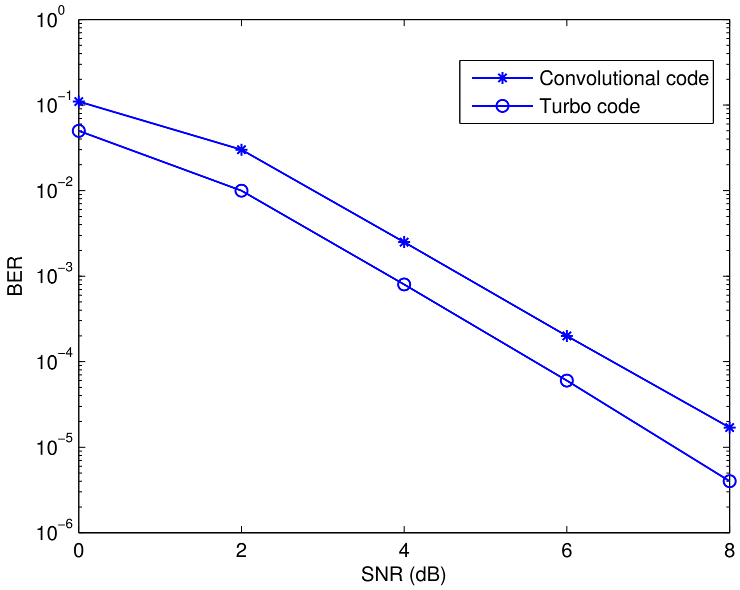

Figure 6. BER performance of the proposed approach at different codes.

It is important to note that the suggested architecture is general in the sense it can be used even in the absence of any relaying transmissions. We simply set $\mathbf{H}_{SRD} = 0$ to disregard the relay link. Figure 7 compares the proposed design's performance with and without AF relaying communications. The findings show that the suggested architecture operates well for non-relaying transmissions and better with AF relaying. The basis for this behavior is because relaying transmissions increases the reliability of the channel decoder outputs, resulting in better performance of the suggested estimator.

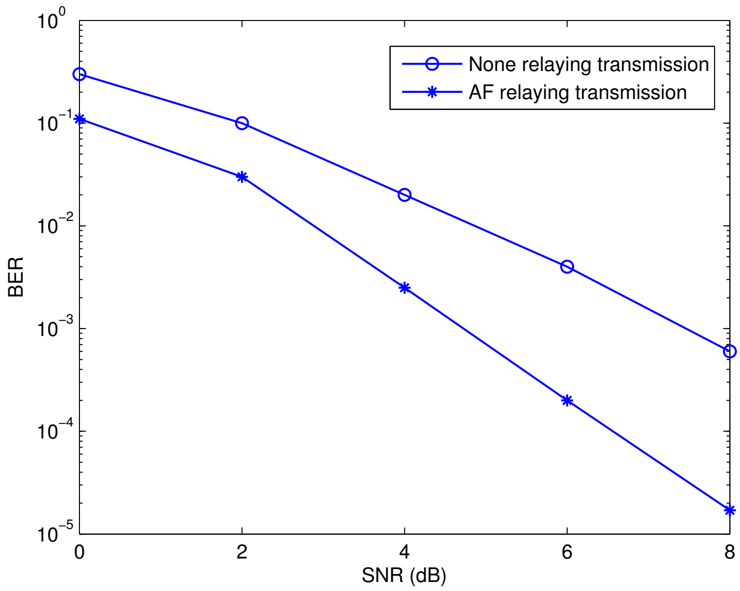

Figure 7. The proposed design's performance with and without AF relaying communications.

Figure 8 illustrates the BER performance of the offered design as a function of the number of receive antennas V at SNR = 4 dB. There is no denying that the number of receive antennas contributes to an improvement in the BER performance. This is because when V increases, the soft information that the decoder produces becomes more reliable. This, in turn, causes an improvement in the quality of the parameter estimation. In addition, the results reveal that there are no significant gaps between the BER performance of the suggested technique and the ideal scenario of having complete information about channel coefficients and IQI parameters.

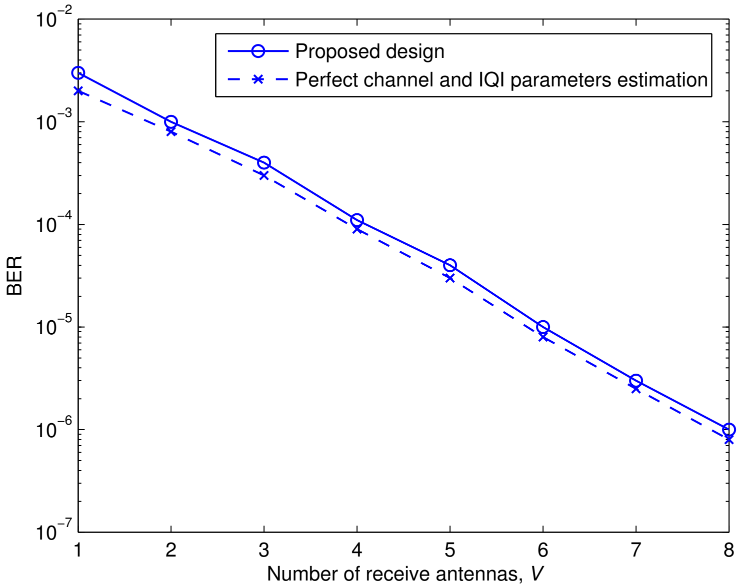

Figure 8. BER performance of the suggested strategy when there are multiple antennas at the destination, SNR = 4 dB.

6. Conclusions

This study underlined the IQI challenge experienced by SC-FDE AF relaying transmissions over unknown wireless channels. We came up with a novel ML strategy for inferring IQI occurring at each terminal along with the wireless multipath channel parameters. An iterative EM procedure was utilized in the process of implementing the offered ML strategy. The estimates were improved by taking advantage of the soft information introduced by the error-correcting decoder. The analysis has shown that it is feasible to estimate the parameters under consideration using a single algorithm, as opposed to employing several independent techniques. In addition, we demonstrated how to make use of the predicted parameters in order to carry out the decoding process. The proposed algorithm is capable of handling both relaying and non-relaying coded transmissions. However, the findings are optimized when relay transmissions are coupled with robust error-control codes. Simulation results reveal that the proposed detector's BER performance when adopted with the offered estimation approach is comparable to that of the ideal case when all parameters are available in advance.

Author Contributions: Conceptualization, M.M. and H.M.; methodology, M.M. and H.M.; software, M.M. and H.M.; validation, M.M. and H.M.; formal analysis, M.M. and H.M.; investigation, M.M. and H.M.; resources, M.M. and H.M.; data creation, M.M. and H.M.; writing—original draft preparation, M.M. and H.M.; writing—review and editing, M.M. and H.M.; visualization, M.M. and H.M.; supervision, M.M. and H.M.; project administration, M.M. and H.M.; funding acquisition, M.M. and H.M. All authors have read and agreed to the published version of the manuscript.

Funding: Princess Nourah bint Abdulrahman University Researchers Supporting Project number (PNURSP2023R137), Princess Nourah bint Abdulrahman University, Riyadh, Saudi Arabia.

Institutional Review Board Statement: Not applicable.

Informed Consent Statement: Not applicable.

Data Availability Statement: Not applicable.

Acknowledgments: The authors would like to acknowledge the support of Prince Sultan University for paying the Article Processing Charges (APC) of this publication.

Conflicts of Interest: The authors declare no conflict of interest.

References

1. Parveen, N.; Abdullah, K.; Islam, M.R.; Abbasi, M.A.K. Performance Analysis Antenna Diversity Technique with Wavelet Transform Using Array Gain for MillimeterWave Communication System. *Electronics* **2022**, *11*, 2626. [CrossRef]
2. Wasim, M.; Khera, S.; Malik, P.K.; Kumari, S.V.; Das, S.; El-Shafai, W.; Aly, M.H. Base Station MIMO Antenna in 1 × 6 Array Configurations with Reflector Design for Sub-6 GHz 5G Applications. *Electronics* **2023**, *12*, 669. [CrossRef]
3. Srikar, D.; Nella, A.; Mamidi, R.; Babu, A.; Das, S.; Lavadiya, S.; Algarni, A.D.; El-Shafai, W. A Novel Integrated UWB Sensing and 8-Element MIMO Communication Cognitive Radio Antenna System. *Electronics* **2023**, *12*, 330. [CrossRef]
4. Suresh, A.C.; Reddy, T.S.; Madhav, B.T.P.; Das, S.; Lavadiya, S.; Algarni, A.D.; El-Shafai, W. Investigations on Stub-Based UWB-MIMO Antennas to Enhance Isolation Using Characteristic Mode Analysis. *Micromachines* **2022**, *13*, 2088. [CrossRef] [PubMed]
5. Tseng, F.S.; Lin, C.T.; Lin, W.L.; Chen, K.Y. Finite-Order Filter Designs of Source and Multiple Full-Duplex Relays for Cooperative Communications in Presence of Frequency- Selective Fading and Inter-Relay Interference. *IEEE Trans. Commun.* **2022**, *70*, 3377–3391. [CrossRef]
6. Biswas, N.; Wang, Z.; Vandendorpe, L.; Mirghasemi, H. On Joint Cooperative Relaying, Resource Allocation, and Scheduling for Mobile Edge Computing Networks. *IEEE Trans. Commun.* **2022**, *70*, 5882–5897. [CrossRef]
7. Rauniyar, A.; Osterbo, O.N.; Hakegard, J.E.; Engelstad, P.E. Secrecy Performance Analysis of Cooperative Nonorthogonal Multiple Access in IoT Networks. *IEEE Sensors J.* **2022**, *22*, 19030–19045. [CrossRef]
8. Shaham, S.; Dang, S.; Wen, M.; Mumtaz, S.; Menon, V.G.; Li, C. Enabling Cooperative Relay Selection by Transfer Learning for the Industrial Internet of Things. *IEEE Trans. Cogn. Commun. Netw.* **2022**, *8*, 1131–1146. [CrossRef]
9. Li, Q.; Hu, R.Q.; Qian, Y.; Wu, G. Cooperative communications for wireless networks: techniques and applications in LTE-advanced systems. *IEEE Wirel. Commun.* **2012**, *19*, 22–29. [CrossRef]
10. Zhang, H.; Pan, G.; Ke, S.; Wang, S.; An, J. Outage Analysis of Cooperative Satellite-Aerial-Terrestrial Networks With Spatially Random Terminals. *IEEE Trans. Commun.* **2022**, *70*, 4972–4987. [CrossRef]
11. Ghosh, S.; Acharya, T.; Maity, S.P. Outage Analysis in SWIPT Enabled Cooperative AF/DF Relay Assisted Two-Way Spectrum Sharing Communication. *IEEE Trans. Cogn. Commun. Netw.* **2022**, *8*, 1434–1443. [CrossRef]
12. Jin, X. Amplify-Quantize-Forward Relay Channel With Quadrature Amplitude Modulation. *IEEE Access* **2022**, *10*, 89445–89457. [CrossRef]
13. Pan, X.; Liu, S.; Yan, S. Nonlinearity-Based Ranging Technique in SC-FDE Communication System With Oversampled Signals. *IEEE Access* **2019**, *7*, 49632–49640. [CrossRef]
14. Qiao, Y.; Li, J.; He, B.; Li, W.; Xin, T. A Novel Signal Detection Scheme Based on Adaptive Ensemble Deep Learning Algorithm in SC-FDE Systems. *IEEE Access* **2020**, *8*, 123514–123523. [CrossRef]
15. Zhang, X.; Xia, Y.; Li, C.; Yang, L.; Mandic, D.P. Complex Properness Inspired Blind Adaptive Frequency-Dependent I/Q Imbalance Compensation for Wideband Direct-Conversion Receivers. *IEEE Trans. Wirel. Commun.* **2020**, *19*, 5982–5992. [CrossRef]
16. Moon, S.M.; Lee, H.L. Dual-Band Direct Conversion Receiver With Additive Mixing Architecture. *IEEE Access* **2022**, *10*, 15436–15442. . [CrossRef]
17. Mach, P.; Becvar, Z. Device-to-Device Relaying: Optimization, Performance Perspectives, and Open Challenges Towards 6G Networks. *IEEE Commun. Surv. Tutorials* **2022**, *24*, 1336–1393. [CrossRef]
18. Hossain, M.A.; Md Noor, R.; Yau, K.L.A.; Ahmedy, I.; Anjum, S.S. A Survey on Simultaneous Wireless Information and Power Transfer With Cooperative Relay and Future Challenges. *IEEE Access* **2019**, *7*, 19166–19198. [CrossRef]
19. Chen, C.C.; Ku, M.L. Carrier Frequency Offset Estimation Bound for OFDM-Based Single Relay Networks With Multipath Receptions. *IEEE Access* **2019**, *7*, 63900–63912. [CrossRef]
20. Zhang, Z.; Long, K.; Vasilakos, A.V.; Hanzo, L. Full-Duplex Wireless Communications: Challenges, Solutions, and Future Research Directions. *Proc. IEEE* **2016**, *104*, 1369–1409. [CrossRef]
21. Abdallah, S.; Salameh, A.I.; Saad, M. Joint Channel, Carrier Frequency Offset and I/Q Imbalance Estimation in Ambient Backscatter Communication Systems. *IEEE Commun. Lett.* **2021**, *25*, 2250–2254. [CrossRef]
22. Cheng, X.; Yang, Y.; Li, S. Joint Compensation of Transmitter and Receiver I/Q Imbalances for SC-FDE Systems. *IEEE Trans. Veh. Technol.* **2020**, *69*, 8483–8498. [CrossRef]
23. Mohammadian, A.; Tellambura, C. RF Impairments in Wireless Transceivers: Phase Noise, CFO, and IQ Imbalance—A Survey. *IEEE Access* **2021**, *9*, 111718–111791. [CrossRef]
24. Sandell, M.; Tsimbalo, E.; Jardak, S.; Uchida, D.; Akita, K.; Yoda, D.; Kawaguchi, T.; Sano, M. Estimation of Wideband IQ Imbalance in MIMO OFDM Systems With CFO. *IEEE Trans. Wirel. Commun.* **2021**, *20*, 5821–5830. [CrossRef]
25. Qi, J.; Aissa, S.; Alouini, M.S. Analysis and compensation of I/Q imbalance in amplify-and-forward cooperative systems. In Proceedings of the 2012 IEEE Wireless Communications and Networking Conference (WCNC), Paris, France, 1–4 April 2012; pp. 215–220. [CrossRef]
26. Qi, J.; Aissa, S.; Alouini, M.S. Impact of I/Q imbalance on the performance of two-way CSI-assisted AF relaying. In Proceedings of the 2013 IEEE Wireless Communications and Networking Conference (WCNC), Shanghai, China, 7–10 April 2013; pp. 2507–2512. [CrossRef]

27. Mokhtar, M.; Gomaa, A.; Al-Dhahir, N. OFDM AF Relaying Under I/Q Imbalance: Performance Analysis and Baseband Compensation. *IEEE Trans. Commun.* **2013**, *61*, 1304–1313. [CrossRef]
28. Li, J.; Matthaiou, M.; Svensson, T. I/Q Imbalance in AF Dual-Hop Relaying: Performance Analysis in Nakagami-m Fading. *IEEE Trans. Commun.* **2014**, *62*, 836–847. [CrossRef]
29. Canbilen, A.E.; Ikki, S.S.; Basar, E.; Gultekin, S.S.; Develi, I. Impact of I/Q Imbalance on Amplify-and-Forward Relaying: Optimal Detector Design and Error Performance. *IEEE Trans. Commun.* **2019**, *67*, 3154–3166. [CrossRef]
30. Gao, Y.; Chen, Y.; Chen, N.; Zhang, J. Performance Analysis of Dual-Hop Relaying With I/Q Imbalance and Additive Hardware Impairment. *IEEE Trans. Veh. Technol.* **2020**, *69*, 4580–4584. [CrossRef]
31. Cheng, H.; Xia, Y.; Huang, Y.; Yang, L.; Mandic, D.P. Joint Channel Estimation and Tx/Rx I/Q Imbalance Compensation for GFDM Systems. *IEEE Trans. Wirel. Commun.* **2019**, *18*, 1304–1317. [CrossRef]
32. Samara, L.; Gouissem, A.; Hamila, R.; Hasna, M.O.; Al-Dhahir, N. Full-Duplex Amplify-and-Forward Relaying Under I/Q Imbalance. *IEEE Trans. Veh. Technol.* **2020**, *69*, 7966–7970. [CrossRef]
33. Marey, M. Solving IQ Mismatch Problem for Two-Path Successive Relaying OFDMA Uplink Systems With Direct Conversion Transceivers. *IEEE Wirel. Commun. Lett.* **2019**, *8*, 33–36. [CrossRef]
34. Marey, M. Soft-Information Aided Channel Estimation With IQ Imbalance for Alternate-Relaying OFDM Cooperative Systems. *IEEE Wirel. Commun. Lett.* **2018**, *7*, 308–311. [CrossRef]
35. Marey, M.; Mostafa, H.; Alshebeili, S.A.; Dobre, O.A. Iterative Modulation Classification Algorithm for Two-Path Successive Relaying Systems. *IEEE Wirel. Commun. Lett.* **2021**, *10*, 2017–2021. [CrossRef]
36. Fernandez, J. Joint Synchronization and Compressive Channel Estimation for Frequency-Selective Hybrid mmWave MIMO Systems. *IEEE Trans. Wirel. Commun.* **2022**, *21*, 548–562. [CrossRef]
37. Marey, M.; Mostafa, H. Autonomous Modulation Categorization Algorithm for Amplify and Forward Relaying Diversity Systems. *Electronics* **2022**, *11*, 1899. [CrossRef]
38. Bedeer, E.; Marey, M.; Dobre, O.; Baddour, K. Adaptive Bit Allocation for OFDM Cognitive Radio Systems with Imperfect Channel Estimation. In Proceedings of the 2012 IEEE Radio and Wireless Symposium, Santa Clara, CA, USA, 15–18 January 2012; pp. 359–362. [CrossRef]
39. M. Marey, H. Mostafa, O. A. Dobre, and M. Ahmed. Data Detection Algorithms for BICM Alternate-Relaying Cooperative Systems with Multiple-Antenna Destination. *IEEE Trans. Veh. Technol.* **2016**, *65*, 3802–3807. [CrossRef]
40. L. Xiang, R. Maunder, and L. Hanzo. Concurrent OFDM Demodulation and Turbo Decoding for Ultra Reliable Low Latency Communication. *IEEE Trans. Veh. Technol.* **2020**, *69*, 1281–1290. [CrossRef]
41. Z. Wu, L. Zhang, and Z. Zhong. A Maximum Cosinoidal Cost Function Method for Parameter Estimation of RSC Turbo Codes. *IEEE Commun. Lett.* **2019**, *23*, 390–393. [CrossRef]